

## NEW CONCEPTS FOR RELATIVE NAVIGATION AT PLANETARY APPROACH

*Rainer Bauske<sup>(1)</sup>, Pablo Muñoz<sup>(2)</sup>, David Lázaro<sup>(3)</sup>, and Stefano Casotto<sup>(4)</sup>*

*<sup>(1)</sup>Terma GmbH, ESOC, HSO-GFS*

*Terma GmbH, c/o European Space Operations Center (ESOC)*

*Robert-Bosch-Str. 5, 64293 Darmstadt, Germany*

*phone: +49 (0)6151 902795*

*email: Rainer.Bauske@esa.int*

*<sup>(2)</sup>GMV, ESOC, HSO-GFS*

*GMV, c/o European Space Operations Center (ESOC)*

*Robert-Bosch-Str. 5, 64293 Darmstadt, Germany*

*phone: +49 (0)6151 902347*

*email: Pablo.Munoz@esa.int*

*<sup>(3)</sup>Space Operations Consulting SL (SOPCO)*

*Space Operations Consulting, SL*

*Paseo General Martínez Campos, 49*

*E-28010 Madrid, Spain*

*phone: +49 151 56118722*

*email: david.lazaro.salvador@spaceoperationsconsulting.com*

*<sup>(4)</sup> Department of Physics and Astronomy, and Center for Space Studies*

*University of Padua*

*Violo Osservatorio 3*

*35122 Padova, Italy*

*phone: +39 049 827 8224*

*email: stefano.casotto@unipd.it*

**Abstract:** *We combined within the ESA orbit determination software new radiometric and optical measurement types with previously existing ones in order to improve the orbital knowledge for celestial body approaches of interplanetary missions. As new radiometric types we introduced Satellite to Satellite/Lander Tracking, Differenced Doppler, and Same Beam Interferometry, as new optical data type Landmarks. Existing types include Range, Doppler, Delta-DOR, and far distance (point) optical data. We address combinations of above measurement types as ‘Navigation Concepts’ and define them specifically as combinations of measurement types complementing each other in terms of required resources, information content, and timing during approach with the goal to find combinations which*

- are feasible for a given mission scenario,*
- offer the highest information content,*
- allow the quickest recovery after loss of orbital knowledge.*

*In selected approach scenarios of BepiColombo, ExoMars, Mars Express and Rosetta we illustrate the applicability of the new measurement types above and compare the advantages of their various combinations in order to find the best navigation concept for the given situation.*

**Keywords:** *Navigation data types, Planetary Approach, Covariance Analysis, Error Ellipsoid.*

## 1. Introduction

In the past ESA mainly used the radiometric measurement types Range, Doppler, and Delta-DOR which provide absolute measurements. Radiometric measurement types not yet used by ESA, hence 'new', include Satellite to Satellite/Lander Tracking, Same Beam Interferometry, which are relative measurements, and Differenced Doppler,

For the approaches of the asteroids Steins (2008) and Lutetia (2010) by the Rosetta spacecraft, ESA employed optical measurements, where the inertial direction (right ascension and declination) from the spacecraft to the target was determined by comparing the position of the asteroid to positions of background stars on images taken by the navigation and science cameras. For point-like targets like these asteroids, the use of defocused images permits the determination of the direction with sub-pixel accuracy. For extended objects, like planets, and especially for the very close approach of Rosetta to comet Churyumov-Gerasimenko a different approach needs to be taken, which uses positions of discernible surface features (landmarks) on camera images. Both optical types provide relative measurements of spacecraft and target body.

All these measurement types have specific information content and a specific demand of resources (number of stations with spacecraft visibility, 2nd spacecraft/lander availability, and on-board cameras). Therefore immediately questions arise such as:

- Which combination of them is feasible for a given mission scenario?
- Which combination offers the highest information content?
- Which combination allows the quickest recovery after loss of orbital knowledge?

In the following we address these combinations of measurement types as 'Navigation concepts' and define them specifically as combinations of measurement types complementing each other in terms of required resources, information content, and timing during a celestial body approach.

The orbital knowledge is determined by observation types, noise and schedule, but not observation values. In order to estimate the knowledge (position covariance matrix) of the spacecraft trajectory during an approach, we implemented a navigation analysis tool consisting of an observation scheduler, a new covariance analysis mode within the ESA orbit determination software, sensitivity analysis tool, and a plotting component. The observations scheduler generates an observations file from a specification of the measurement schedule, measurement models and parameters, stations, landmarks, orbit file, and other inputs. It accounts for the visibility of spacecraft and selected quasars from scheduled stations, and for the visibility of landmarks, lander, or another spacecraft from the spacecraft. The resulting observation file contains type, time and properties of the possible observations. It is fed into the orbit determination software, which in the new mode performs only the first iteration of the orbit determination process including the computation of partial derivatives to return a solution file with the epoch state a posteriori error covariance (ellipsoid) at the state epoch. The error ellipsoid can be projected on the target body's B-plane (miss vector position uncertainty) and its normal (representing arrival time uncertainty). The navigation analysis tool allows in this way to set up experiments in order to examine the resulting orbital knowledge of a given orbit determination scenario for missions like Mars Express (MEX), ExoMars (EXM), Rosetta (ROS), and BepiColombo (BC) as shown below. For details on software and all experiments refer to [1].

## 2. Measurement types

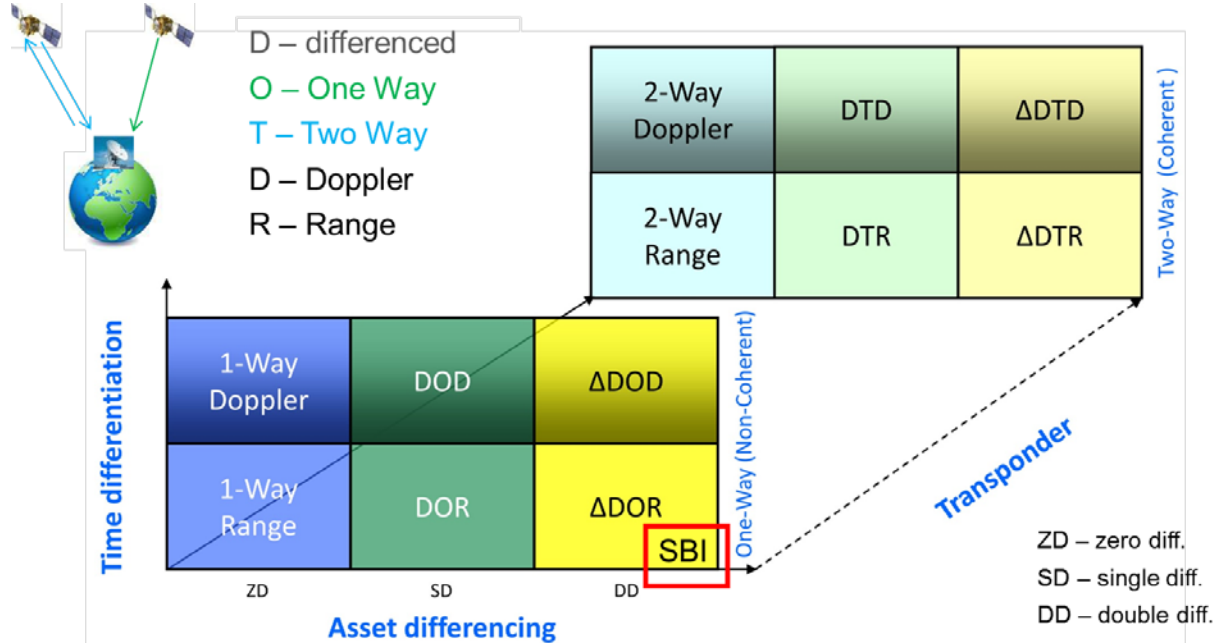


**Figure 1. Radiometric Measurement Types Displayed According to (i) Differencing in Time, (ii) Differencing in Assets, and (iii) Coherency**

Fundamental radiometric data types can be distinguished by three characteristics as shown in Fig. 1. The first characteristic is time differencing, shown in the vertical axis. Accordingly, measurements are either of type Range or of type Doppler. The second characteristic is the number of transmitting and observing assets involved in the measurement. If only one transmitter and one observer are involved, then the observation is un-differenced. If one transmitter and two observers are involved, then the observation is differenced. If two transmitters and two observers are involved, then the measurement is a Delta differenced measurement. The third discriminating characteristic is the presence of a transponder on the space asset. This makes measurements either one-way or two-way. One-way measurements are also known as non-coherent measurements, while two-way measurements are known as coherent measurements. The measurements listed in Fig. 1 are Range, Doppler, Differenced Range, Differenced Doppler, Delta Differenced Range and Delta Differenced Doppler, in both coherent and non-coherent flavors. Here we do not split further into different technical implementations, i.e. ESA and NASA Doppler types, but at software level (definition of measurements) they are treated differently.

### Differenced RANGE Measurement Model (DOR, DTR)

Differenced range measurements can either be coherent, when two-way measurements are involved, or non-coherent, when one-way measurements are involved. The Differenced One-way Range (DOR) measurement type involves two ground stations at  $r_1$  and  $r_2$  taking one-way down-range measurements  $\rho_1$  and  $\rho_2$  which are then subtracted one from the other to form the difference  $\Delta\rho = \rho_1 - \rho_2$ . The coherent version is formed by the same differencing process, except in this case one of the stations transmits the uplink signal which is then transponded back at the spacecraft to the two stations. This case is termed Differenced Three-way Range (DTR).

### **Differenced DOPPLER Measurement Model (DOD, DTD)**

The Differenced Doppler data type can be built as the difference between a two-way Doppler measurement and a three-way Doppler measurement originating at the same ground station [3]. In this case we refer to Differenced Doppler as Differenced Two-way Doppler (DTD), a coherent data type. Since differencing effectively eliminates the uplink transmission segment, Differenced Doppler is nominally equivalent to singly differenced downlink Doppler, which we refer to as Differenced One-way Doppler (DOD), a non-coherent data type. Of course, if both ground stations transmit a carrier, that makes Differenced Doppler a dual measurement type, i.e., Differenced Doppler is collected at both ground stations during the common pass. It is also possible to build Differenced Doppler as the difference between two three-way Doppler measurements, in which case one station acts as the transmitter and two ground stations as the receivers. Its advantages are:

- Competitive with more cumbersome  $\Delta$ DOD (no antenna steering required)
- Near real time data availability (no correlator needed)

Its disadvantages are:

- Needs station clock synchronization within or better than 1 ns (e.g. GPS-enabled)
- Singular Declination (DEC) on equator
- No sensitivity to range (only to Right Ascension (RA) and Declination)

### **Delta Differenced RANGE Measurement Model ( $\Delta$ DOR, $\Delta$ DTR)**

When we apply the DOR scheme to two sources  $s_1$  (the S/C) and  $s_2$  (the Quasar, or other asset) which are close to each other, we can express the coordinates of the second in terms of the first, expand the second DOR measurement about the first, difference them and achieve an approximate Delta Differenced One-Way Doppler ( $\Delta$ DOR) measurement model. In inter-planetary navigation it is often used because of its high accuracy and because it has no DEC singularity in its covariance matrix. Its major disadvantage is that it needs short term steering of the antenna, switching between quasar Q and Spacecraft S in sequences such as Q-S-Q, S-Q-S.

### **Same Beam Interferometry (SBI) Measurements**

In the Same-Beam Interferometry technique each ground tracking station simultaneously receives signals from a pair of space assets, where we assume a spacecraft already orbiting (could be also a lander) and a navigating spacecraft approaching a Solar System body. The tracking data are then differenced between receivers and between assets, which eliminates all common-mode errors and disturbances, when the appropriate corrections are applied in order to synchronize the stations timescales. Both signals are assumed to be simultaneously recorded at two receiving ground stations. The basic observable at each ground station is a one-way Doppler observable. Thus, SBI is a non-steering variant of  $\Delta$ DOR where two sources are observed within the same RX antenna beam width. It has not yet been adopted by ESA, but there were successful experiments by JPL. SBI has the advantages of Real Time processing (no latency) and total cancellation of clock errors, but it needs more sophisticated signal processing and a large capacity telemetry communication channel – and of course two assets within the antenna beam width.

### **Spacecraft-Spacecraft and Spacecraft-Lander One Way Doppler**

Additional relative radiometric types are the Spacecraft-Spacecraft and the Spacecraft-Lander tracking types which are distinguished by the connection to the rotational state of a body in the

latter case. Both types are distinguished from traditional Earth based radiometric tracking because simplifications done in [2] to describe the information content of the traditional radiometric tracking do not apply, mainly because the geometry of the measurements during the integration in time now depends on both participants.

### Optical Measurement Types

In principle different optical types could be defined based on the image source (star tracker image with several known point sources versus body surface image with one or several locations connected to the surface state of one body). However, after pre-processing these differences do not result in a different treatment within the software, therefore only two optical types are distinguished: Optical images for pointing to the body center, which we also call Distant Target Pointing (DTP), and optical images for features in the surface (Landmarks). Internally, the DTP processing contains a solution of the light time equation until the body is close enough, that it can be neglected.

#### 2.1. Information Content and Required Resources

Table 1 shows the information content, and the required resources of each available measurement type. In the table  $r$ ,  $v$ ,  $\delta$ ,  $\alpha$  are the S/C radius (S/C-Earth distance), velocity (S/C-Earth distance rate), declination, right ascension in the Earth-Centered Inertial reference frame (ECI). For relative observations,  $d\delta$  and  $d\alpha$ , are angles w.r.t. right ascension and declination a-priori values,  $dv \cdot t$  is the distance to the assumed plane of an image (e.g. for fly-bys  $dv$  as relative velocity perpendicular towards the target plane and  $t$  the time until closest approach, which is the ‘arrival’ in the target plane),  $dt$  the variation of this arrival time.

When the S/C is far away from the target body of a flyby, the right ascension and declination of the body is much better determined than the distance from the S/C to the body. Landmark observations take place when the S/C will be relatively close to the body. In general, the landmarks observables provide the same information content as the pointing to the body (that is right ascension and declination of the body as seen from the S/C), and additionally, they provide information on body rotational state (north-pole direction  $p_x$ ,  $p_y$ ,  $p_z$ , rotation phase  $\phi$  wrt. to prime meridian) and better information in the S/C-body distance  $dz$ .

**Table 1. Measurement Types**

Type	Name	Information Content	Exclusion	Resources	Data sources supported by Nav. Analysis Tool
				Transmitter /Observer /Transponder /Other	ESA/NASA (E/N)
OWR	1-Way Range	$r, \delta, \alpha$	$\delta=0,90$	1/1/0	E/N
TWR	2-Way Range	$r, \delta, \alpha$	$\delta=0,90$	1/1/1	E/N
OWD	1-Way Doppler	$v, \delta, \alpha$	$\delta=0,90$	1/1/0	E/N
TWD	2-Way Doppler	$v, \delta, \alpha$	$\delta=0,90$	1/1/1	E/N
THWD	3-Way Doppler	$v, \delta, \alpha$	$\delta=0,90$	1/2/1	-

Type	Name	Information Content	Exclusion	Resources	Data sources supported by Nav. Analysis Tool
DOR	Differenced 1-Way Range	$\delta, \alpha$	$\delta=90$	1/2/0	E/N
DTR	Differenced 2-Way Range	$\delta, \alpha$	$\delta=90$	1/2/1	-
DOD	Differenced 1-Way Doppler	$\delta, \alpha$	$\delta=90$	1/2/0	E
DTD	Differenced 2-Way Doppler	$\delta, \alpha$	$\delta=90$	1/2/1	-
dDOR	Delta-DOR	$\delta, \alpha$	$\delta=90$	1/2/0/quasar	E/N
dDTR	Delta-DTR	$\delta, \alpha$	$\delta=90$	1/2/1/quasar	-
SBI	Same-Beam-Interferometry	$\delta, \alpha$	$\delta=90$	2/2/0/ 2nd S/C	E
SBI2	2-Way SBI	$\delta, \alpha$	$\delta=90$	2/2/2/ 2nd S/C	
SST	Spacecraft-Spacecraft Tracking (OWD)	$dv, d\delta, d\alpha$	$d\delta=0, 90$	1/1/0/ 2nd S/C	E
SLT	Spacecraft-Lander Tracking (OWD)	$dv, d\delta, d\alpha$	$d\delta=0, 90$	1/1/0/ Lander	E
DTP	Distant Target Point (Body center pointing)	$d\delta, d\alpha, dv*dt$		Camera	E
LMK	Landmark	$d\delta, d\alpha, dz, px, py, pz, \varphi,$		Camera	E

### 3. Navigation Concepts

The observations types can be grouped in terms of their information content and their expected applicability for different approach phases:

General:

- Earth Line of Sight (LOS): Range, Doppler.
- Plane Normal to Earth LOS: Delta-DOR, SBI, Differenced Doppler

Far approach:

- Target Body LOS: S/C-S/C (or Lander) Tracking
- Normal to Target Body LOS: Optical Images (DTP)

Close approach:

- Landmarks, S/C - Lander Doppler: Information on trajectory of S/C w.r.t body surface.
- S/C - S/C: Information on spacecraft relative trajectory (depend on orbits' geometry)

Based on this, navigation concepts that theoretically combine the observations' information content can be defined, using Range and Doppler as a baseline:

Far approach to a planet (well known body ephemerides):

- Range, Doppler, Delta-DOR
- Range, Doppler, Diff. Doppler
- Range, Doppler, Optical Images (DTP), S/C-S/C Tracking

Close approach to a planet (like the case of an insertion arc or the initial orbit):

- Range, Doppler, Delta-DOR
- Range, Doppler, SBI
- Range, Doppler, Landmarks (pre-existing catalogue of landmarks should be available)
- Range, Doppler, S/C-Lander Doppler
- Range, Doppler, S/C-S/C Doppler
- Range, Doppler, Diff. Doppler

Approach to Small body (neither well known properties, nor S/C or lander around target body):

- Range, Doppler, Delta-DOR, Optical Images (DTP)
- Range, Doppler, Diff Doppler, Optical Images (DTP)

Around Small body (Not well known properties. Interest mainly in relative state, thus no Delta-DOR, SBI, Diff Doppler):

- Range, Doppler, Landmarks
- Range, Doppler, Landmarks, S/C Lander -> assuming lander already delivered

#### **4. Modeling of Spacecraft Dynamics**

Orbit Control Maneuvers (OCM), Wheel-Off-Loading Maneuvers (WOL), and Safe Modes (SFM) affect the orbit via forces and the orbital knowledge by uncertainties in onset time, duration, magnitude and direction of the applied forces. Depending on the type of S/C, balanced (ROS) or unbalanced (MEX) Wheel-Off-Loading maneuvers may take place, where unbalanced ones add a small delta-v to the orbit, and both types add to the uncertainty. They are formulated as impulsive maneuvers. Orbit control maneuvers are used for targeting. They are defined as non-impulsive thrust arcs with either inertial constant thrust direction or as vectored maneuvers. The latter have been used for orbit insertion of Mars Express. The chemical propulsion system of the Mercury Planetary Orbiter Composite during the insertion is modeled as a thrust ramp with 500 s duration from 10 to 100% of thrust and a consecutive burn firing phase with constant thrust at 100%. Spacecraft separations, i.e. for lander deliveries are treated like impulsive maneuvers. Safe modes are seen here as stochastic thrust arcs with unknown direction, duration and delta-v which also interrupt the S/C communication and lead to loss of orbital knowledge.

#### **5. Mars-Express Close Approach - Short Observation Interval after Save Mode**

The Mars approach of Mars Express acts as an example to establish basic properties of the data types on the background of a real mission. Data of the Mars Express approach before the orbit insertion maneuver are complicated by the occurrence of a safe mode 17 days before the lander delivery, scheduled unbalanced wheel-off-loadings and the lander delivery itself. Mars, however, is more likely to allow future possibilities for S/C-S/C and S/C-lander tracking. Excluding the dust-storm season, its atmosphere allows use of landmarks for planetary approaches. Therefore we re-used data from the Mars Express approach and current operational settings in our scenarios and augmented them with data/assets required for the new data types. To allow experiments using SBI and S/C-S/C Doppler data we assumed a 2nd spacecraft “orbiter” already in orbit at Mars with orbital elements (Mars Mean Equator system) corresponding to recent values of Mars Express (June 2012) but with predated time, as shown in Table 2. In order to allow experiments with optical data, we also assumed a navigation camera with properties of the Rosetta NAVCAM taken from [9], see Table 3. We analyzed observation arcs of different lengths, establishing

sensitivities of the various data types with respect to their parameters, their applicability for the given scenario and the resulting B-plane and arrival time errors of their combinations. The data types involved were Range, Doppler, DDOR, S/C-S/C Doppler, optical images (DTP and Landmarks), and Same Beam Interferometry.

**Table 2. State Elements of Assumed Mars Orbiting Spacecraft**

Element	Value
Time	2003/10/22_00:00:00.0000 (UTC)
Pericenter radius	3702.1335157 km
Apocenter radius	13944.4652253 km
Inclination	86.8700885712 deg MME
Right Ascension of ascending node	11.1738707214 deg MME
Argument of pericenter	-86.2188569673 deg MME
True Anomaly	-15.1497773527 deg

**Table 3. Properties of the Rosetta Cameras**

	NAVCAM	SCICAM (OSIRIS Narrow Angle)	SCICAM 2 (OSIRIS Wide Angle)
Sensitivity	11 mag	> 15 mag	
Field of view [deg]	5x5	2.2x2.2	11x11
Pixels	1024x1024	2048x2048	2048x2048
Resolution (bit/pixel)	12	16	16
Pixel angular resolution [mdeg]	5	1.1	5.8

### 5.1. Schedule

Mars Express went into Safe Mode on December 02, 2003 which seriously degraded the prediction accuracy. According to [4], by December 08 the orbital knowledge had largely been regained. Figure 7 of [4] shows a comparison of B-plane ellipse estimates for December 23 obtained with Range, Doppler, Delta-DOR and combinations of them. In order to produce a similar case we used as approach schedule the deterministic maneuvers as predicted by the optimization of 2013/11/09 which was used to determine the TCM 3 maneuver, see Table 4. For the observations we used the following schedule:

- A-priori state taken at 2003/12/08 with Sigma 50 km, 5m/s (assuming regained knowledge) in position and velocity components, respectively.
- Observation interval: 2003/12/09 – 2003/12/23.
- ESA-2-Way Range: X-band, Sampling rate 1200 s; ESA-2-Way Doppler: X-band, Sampling rate 60 s, Doppler Count time 60 s; Both with minimum elevation = 15.0 deg, pass duration = 6.0 h, station New Norcia.
- DSN-DeltaDOR: Quasar 24, Pass frequency 2, baseline 1 with stations Goldstone and Madrid, baseline 2 with stations Goldstone and Canberra.
- Differenced Doppler: sampling rate 60 s, count time 60 s, maximum pass duration 6 h, stations New Norcia and Cebreros.
- Optical images (DTP): Sampling rate 2 h, 3 images per time batch.

- S/C-S/C tracking: Observations were scheduled between 2003/12/18 and 2003/12/22 for 2 hours per day with sampling rate and count time set to 60 s. This assumes limitations caused by schedules of the tracking S/C.

**Table 4. Schedule of MEX Mars Approach (from Optimization MEX 031109\_001)**

Maneuver	Date [MJ2TDB]	Date [TDBCAL]	Delta-V [m/s]	Duration [s]
Unscheduled Safe Mode on December 02				
OCM WOL_3_Dec	1432.338879	2003/12/03_08:07:59.183	0.01561397	0.460
OCM WOL_10_Dec	1439.328984	2003/12/10_07:53:44.183	0.01941081	0.572
OCM WOL_15_Dec	1444.315963	2003/12/15_07:34:59.183	0.00998458	0.294
LANDER EJECTION	1448.341831	2003/12/19_08:12:14.184	0.01809895	
OCM WOL_19 <sup>th</sup> _Dec	1448.386622	2003/12/19_09:16:44.182	0.0306297	0.850
OCM RETARGETING MAN.	1449.340771	2003/12/20_08:10:42.627	5.60459706	155.448
OCM WOL_23 <sup>th</sup> _Dec	1452.265442	2003/12/23_06:22:14.184	0.01530606	0.424
OCM CAPTURE MANEUVER	1454.128148	2003/12/25_03:04:32.002	807.1220736	2043.130
<b>Capture</b>			<b>Pericenter radius [km]</b>	<b>Inclination [deg]</b>
Closest approach	1454.131107	2003/12/25_03:08:47.685	3821.125164	7.912

## 5.2. Applicability of Observation Types

The first question is always, which observation types can be used, i.e. their applicability for a given scenario:

**Range and Doppler:** Conventional 2-way, X-band Doppler and Range data were acquired during daily passes of New Norcia. The Doppler data were compressed to 60 s count time.

**Delta-DOR:** During November 10 and December 24 overall 105 Delta-DOR data points were produced from the NASA/DSN network using baselines Goldstone-Madrid (E-W) and Goldstone-Canberra (N-S) and one of four quasars. The frequency of the data points increased towards the end of this period. We assumed a simpler schedule with measurements (S-Q-S) taken every 2<sup>nd</sup> pass to achieve similar numbers of observations in the observation interval considered below. We also established that the Delta-DOR results had a negligible dependence on which of the nearby quasars was selected in comparison to differences wrt. other data types and used only one Quasar.

**Differenced Doppler:** For Differenced Doppler data, two ground stations need to be available during an observation pass. We used the station New Norcia and assumed Cebreros to be available as well.

**SBI:** For ESA ground stations the beam-width is 70 mdeg in the X-band. With this beam-width SBI data will become available 2003/12/24 04:00:00 (1453.16 MJD2T), only one day before the capture maneuver, which is too late for commanding of this maneuver as can be seen in Fig. 2.

**S/C-S/C Doppler:** Assuming that for carrier tracking there is no upper limit apart from the power of the S/C sender, there will also be no limit to the maximum distance for relative

tracking. Limits are then given by the mutual visibility of the S/C (occultation margin angle > 0 w.r.t. orbited planet and moons) and the schedule of the tracking S/C.

**Optical Image for Pointing to Body Center (DTP):** Given the sensitivity of 11 magnitudes of the assumed navigation camera, Mars will be visible during the whole approach period and (unless blinding affects the camera) the images could be used as long as the phase angle is small enough to reliably estimate the center of the planet. In Figure 3 the magnitude of Mars as seen by the approaching spacecraft is computed according to  $m = -1.51 + 5 \cdot \log_{10}(r \cdot R) + 0.016 \cdot FV$ , where FV is the phase angle in deg, r is the heliocentric distance of Mars and R the distance Mars to probe, both in AU (source: <http://www.stjarnhimlen.se/comp/ppcomp.html>). The field of view of the Rosetta NAVCAM is 5x5 deg. Mars will fill it on 2003/12/24, 20:00. This will be the latest applicable date for an approach scenario.

**Landmarks:** Assuming that landmarks can be used once the apparent size of Mars as seen from MEX is greater than about 100 pixels  $\approx 0.5$  deg, the minimum distance between Mars and MEX is  $D_{min} = \text{Diameter}_{Mars} / \sin(0.5 \text{ deg}) \approx 780,000 \text{ km}$ . So landmarks could start to be used on 2003/12/21 22:00:00.000 (=1450.9167 MJD2T). We assumed that landmarks can be used where the zenith angles of the landmark-Sun direction as well as of the Landmark – S/C direction are smaller than 70 deg. This corresponds to a Sun-Mars-S/C angle of roughly  $2 \cdot 69 = 138$  deg at the limit. As shown in Figure 3, the phase angle of Mars as seen from the approaching spacecraft increases from 60 up to about 84 deg one day before the capture maneuver, then it drops and increases rapidly, while MEX swings across the dayside towards the night side. This means that for the approach scenarios landmarks can be used after the date indicated above, but not before (and of course not in the planetary shade). This is too late to be useful for commanding of the capture maneuver.

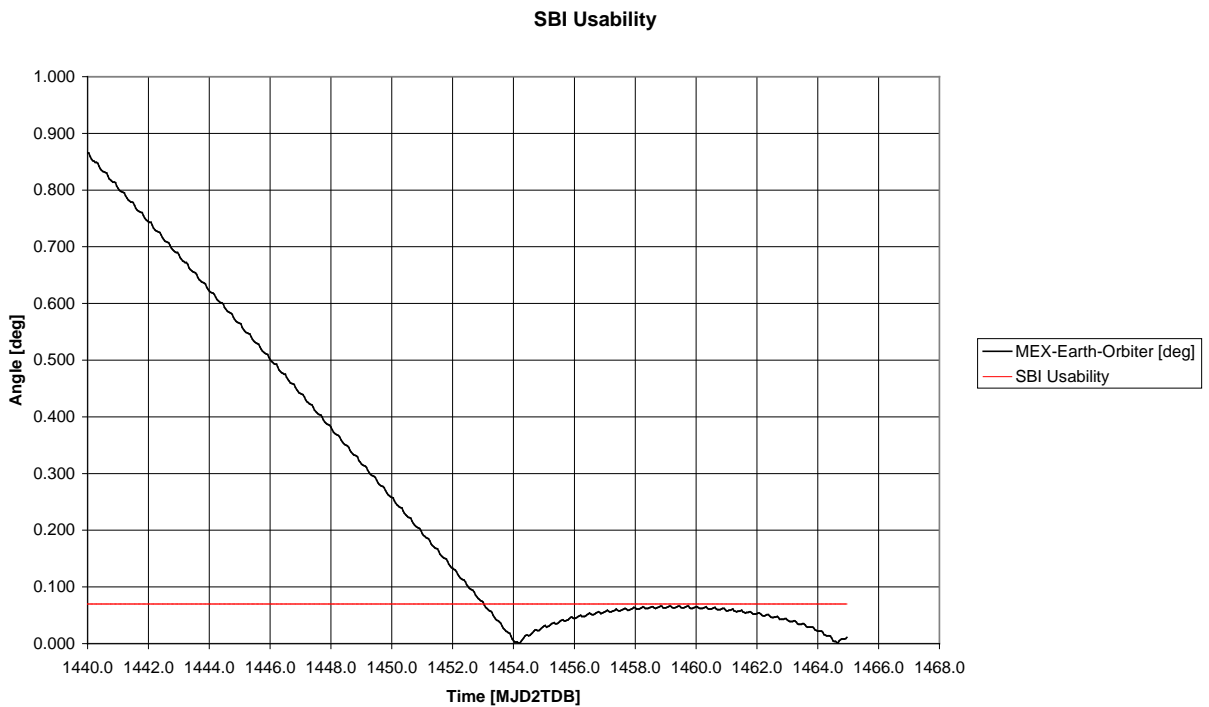


**Figure 2. Usability of SBI Data (MEX)**

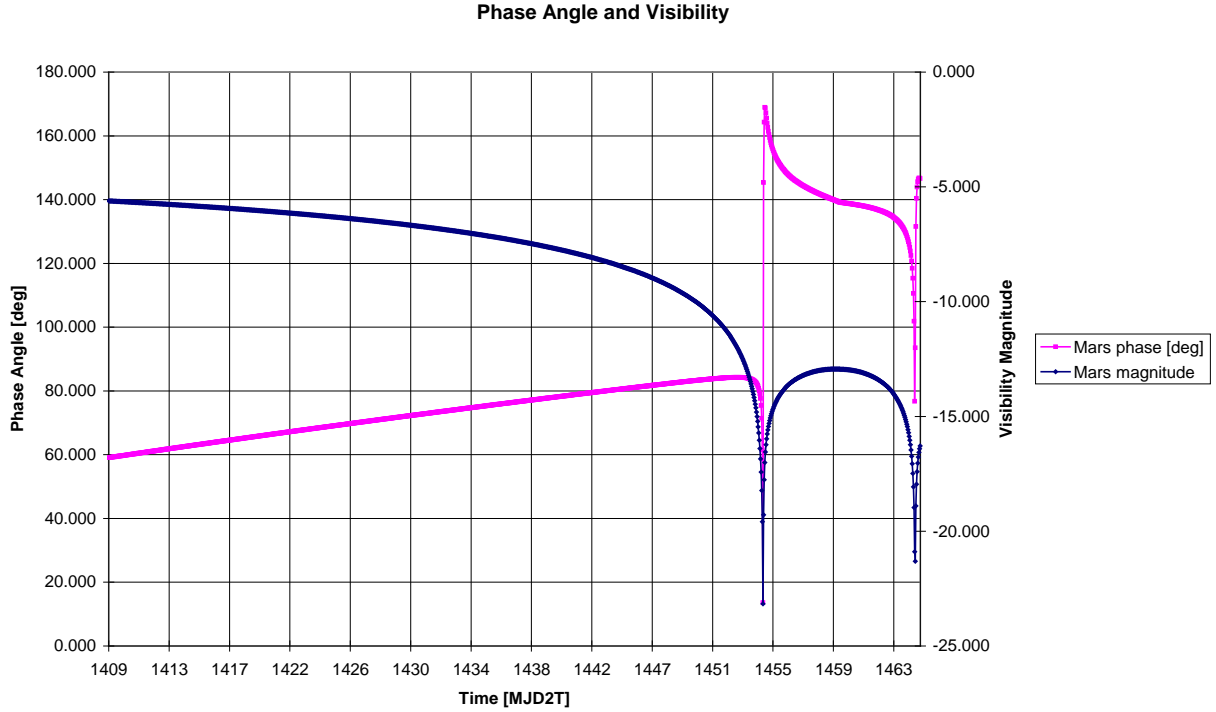


**Figure 3. Visibility of Mars as seen from MEX during Approach**

### 5.3. Models and Parameters

#### Uncertain OD Parameters

Only maneuvers before the data cut-off are included as solve for (Typ S), here the ones from November 10 to December 20, while maneuvers thereafter are taken as exact. The solar radiation pressure is also set as solve for. Unless written otherwise, consider parameters (Typ C) are switched off. When switched on, we assume the uncertainties given in Table 5. Values in Table 6 are uncertainties of observations which are used as inputs for the observation scheduler. We re-use values of this table also for other experiments in this paper.

**Table 5. Uncertain OD Parameters (MEX)**

OD parameter	Typ	A priori value	1 $\sigma$ a priori uncertainty
spacecraft state at epoch	S	taken from optimization 031109_001	50 km, 5 m/s
SRP scale coefficient	S	+ 0 %	5 %
TCM, WOL	S	as commanded	3 % of acceleration for each direction in EME2000 frame (using acceleration file of optimisation)
ESA stations location	C	0	10 cm in each direction
DSN stations location	C	0	as given in [5]
quasar directions	C	0	as given in [6]

OD parameter	Typ	A priori value	1 $\sigma$ a priori uncertainty
Troposphere calibration (zenith delay)	C	0	4 cm (wet part) 1 cm (dry part)
ionosphere calibration scale factor	C	+ 0 %	25 %
Mars ephemeris position, velocity	C	0	1 km, 0.01 mm/s
Mars gravity constant $\mu$	C	0	0.01 km <sup>3</sup> /s <sup>2</sup>
Image calibration bias	C	0	0 for DTP

**Table 6. Default Inputs for Observation Types (MEX)**

ID	Observation type	Type of Noise	Noise level		Converted	
1	IFMS two/three way Range	Range noise	1.67E-008	Sec	5.0	m
2	IFMS two/three way Doppler	Doppler noise	6.67E-013		0.2	mm/s
3	IFMS two/three way ramped Doppler	Doppler noise	6.70E-013		0.2	mm/s
4	IFMS one way Doppler	Doppler noise	1.00E-012		0.3	mm/s
5	DSN one way Doppler f-one	Doppler noise	1.00E-012		0.3	mm/s
6	DSN sequential two-way Range (sra)	Range noise	1.67E-008	Sec	5.0	m
7	DSN two-way Doppler (f-two)	Doppler noise	6.70E-013		0.2	mm/s
8	DSN delta-dor (s/c and quasar)	Dor sigma	6.00E-002	nSec		
10	ESA delta-dor (s/c and quasar)	Dor sigma	2.50E-001	nSec		
16	IFMS Differenced Doppler	Differenced Doppler noise	(8.33E-013) 6.67E-14		(0.25) 0.02	mm/s
17	IFMS same beam interferometry	Sbi noise	1.00E-010		30.0	mm/s
18	S/C to s/c one way Doppler	Doppler noise	1.00E-010		30.0	mm/s
19	S/C to lander one way Doppler	Doppler noise	1.00E-010		30.0	mm/s
14	Optical navigation					
	Right ascension	Standard deviation	1.00E-003	Deg	2	Pixels
	Declination	Standard deviation	1.00E-003	Deg	2	Pixels
	Correlation coefficient:	Ra and dec	0.00E+000	Deg		
15	Optical landmarks navigation					
	Right ascension	Standard deviation	4.80E-003	Deg		
	Declination	Standard deviation	4.80E-003	Deg		
	Correlation coefficient:	Ra and dec	0.00E+000	Deg		

#### 5.4. Reference Results: Range, Doppler, DSN-Delta-DOR

Two experiments are performed, comparing B-plane uncertainty ellipse parameters with and without consider parameters for the standard data types Range, Doppler, Delta-DOR and their combinations, where the consider parameters are set as in Table 5, and with the remaining future wheel-off-loading maneuvers also set as consider for the acceleration components. The number of observations produced by the observation scheduler is: Range 252, Doppler 5054, Delta-DOR 14. Results are in Figure 4 and Table 7. They show that the introduction of Delta-DOR

leads to a reduction of the semi-major axis errors by factors between 3 and 4 w.r.t. the Range-Doppler combination. The effect on the arrival time error is smaller but still above a factor 2.

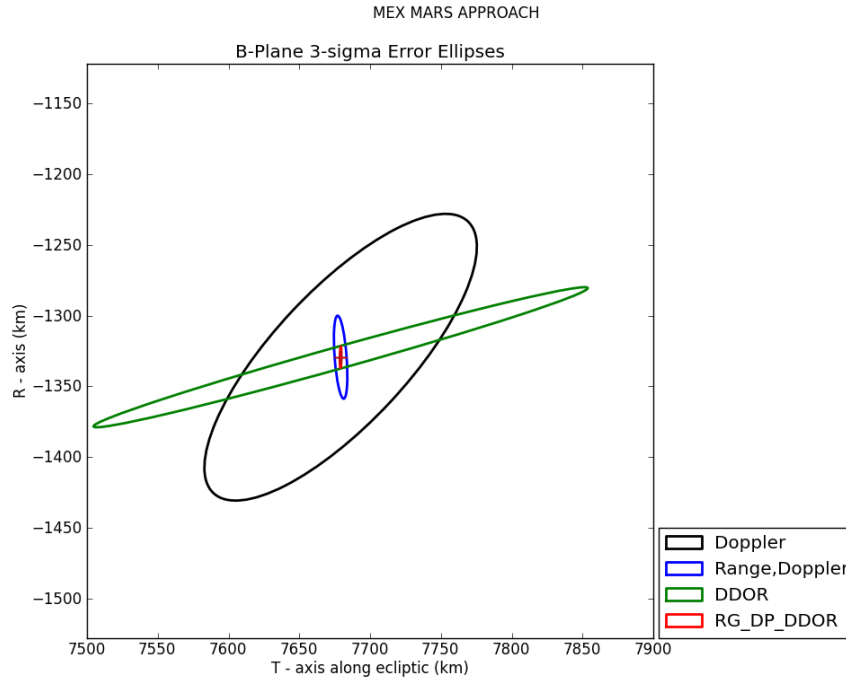


**Figure 4. B-Plane Ellipses of Basic Data Types without Consider Parameters (MEX)**

**Table 7. Reference,  $3\sigma$  Uncertainty Ellipse Parameter (MEX, Short Observation Arc)**

Data type	Semi major axis [km]	Semi minor axis [km]	Arrival time [s]
<b>Without Consider Parameters</b>			
Doppler	131.6	47.3	38.7
Range, Doppler	29.5	4.2	3.7
DSN-DeltaDOR	181.3	7.7	99.4
All combined	7.5	0.5	1.0
<b>With Consider Parameters</b>			
Doppler	131.9	48.8	38.8
Range, Doppler	31.6	5.6	4.0
DSN-DeltaDOR	181.3	9.1	99.4
All combined	9.1	3.4	1.7

### 5.5. Comparison of Navigation Concepts

The concepts we tried are:

- Range + Doppler + Delta-DOR
- Range + Doppler + Diff. Doppler
- Range + Doppler + Optical Images (DTP)
- Range + Doppler + S/C-S/C Tracking
- Range + Doppler + Diff. Doppler + S/C-S/C Tracking
- Range + Doppler + Optical Images + S/C-S/C Tracking

Here we show only cases without consider parameters. The number of observations produced by the observation scheduler is: Range 252, Doppler 5054, Delta-DOR 14, DTP 169, Diff. Dopp. 1235, S/C-S/C 605. Results are shown in Table 8 and Figure 5.

The combination Range + Doppler + Delta-DOR provides the smallest errors, followed by combinations involving S/C-S/C data. In comparison to Range-Doppler, both, DTP and differenced Doppler data reduce the semi-major axis error by a factor of nearly 2 and also reduce the arrival time error considerably. Differenced Doppler data are only slightly worse than DTP. We noted that within alternative concepts (not involving DDOR) the S/C-S/C type lead to the fastest error improvement in experiments varying the duration of the observation arc.

**Table 8. B-Plane  $3\sigma$  Uncertainty Ellipse Parameters (MEX, Short Observation Arc)**

Data Type Combination	Semi Major axis [km]	Semi Minor Axis [km]	Arrival Time [s]
Range+Doppler+Delta-DOR	7.474	0.546	1.032
Range+Doppler	29.458	4.223	3.749
Range+Doppler+Diff. Dopp.	16.926	3.491	2.279
Range+Doppler+ S/C-S/C	9.337	2.193	1.203
Range+Doppler+DTP	16.703	3.174	2.168
Range+Doppler+Diff. Dopp.+S/C-S/C	8.331	2.093	1.098
Range+Doppler+DTP+ S/C-S/C	8.537	2.110	1.108

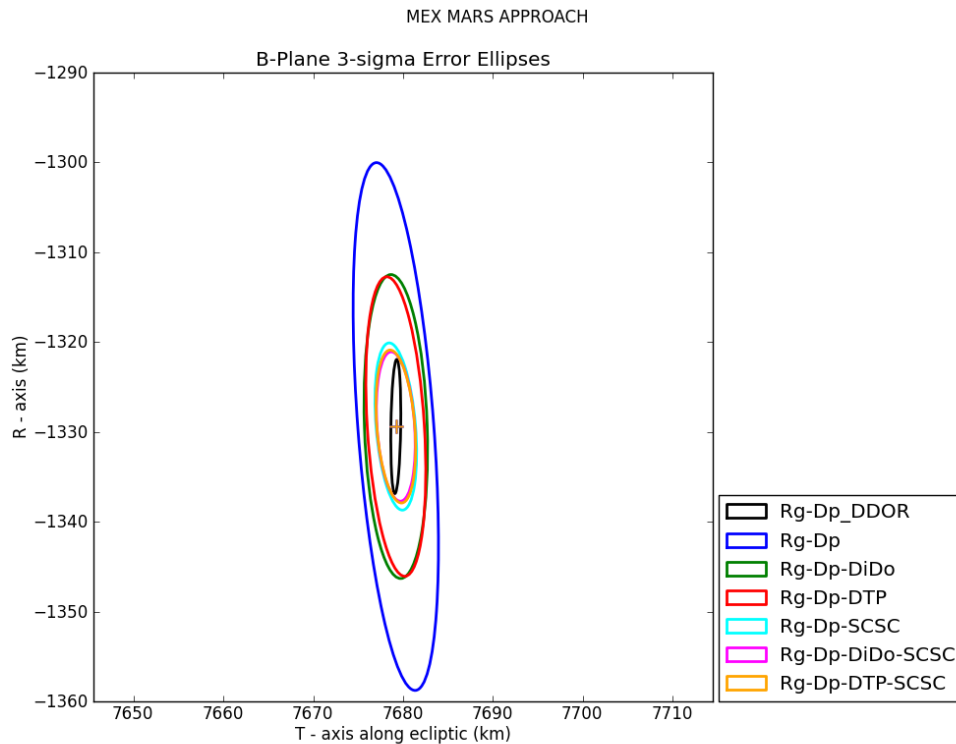


**Figure 5. B-Plane Ellipses of Navigation Concepts for MEX without Consider Parameters**

## 6. ExoMars EDM Separation

The covariance analysis covers the last orbit determination that will be done to command the EDM separation sequence. The observation arc includes a stochastic maneuver slot 5 days before separation. The scenario uses the orbit and acceleration file from optimization LWO\_PROTON\_LAU\_TGO\_WALK\_IN, which represents the current operational modeling of the Mission Analysis results of [7]. Table 9 gives the schedule of the ExoMars mission up to the EDM Separation. For the optical observations we assumed that the spacecraft carries a camera with similar characteristics as Rosetta’s navigation cameras (see Table 3). For SBI we assumed a 2<sup>nd</sup> S/C to be available, but this time we did not simulate the S/C-S/C data type.

### 6.1. Schedule

- Observation interval: 2016/10/08\_12:00 - 2016/10/15\_11:00. Data cut-off is taken 24 hours before separation event. Observation start time is taken such that the whole observation arc is 7 days (longer observations arcs were also tested and resulted in too small uncertainties).
- The observation arc includes a stochastic maneuver slot 5 days before separation. This maneuver is not included in the optimization, since its purpose is to correct for trajectory errors, and thus its size will be defined in-flight. From [7] a delta-V of 50 mm/s (1-sigma) for this maneuver can be expected. Therefore, the maneuver is modeled with zero nominal delta-V and a 1-sigma uncertainty of 1.5 mm/s in each component (3% of maneuver magnitude).
- The S/C orbit a-priori state is taken at the beginning of the arc, 2016/10/08\_13:00, with very big uncertainties so that the run results represent the amount of information obtained from the measurements.
- ESA-2-Way Range: X-band, sampling rate 1200 s; ESA-2-Way Doppler: X-band, sampling rate 60 s, Doppler count time 60 s; Both with minimum elevation = 15.0 deg, pass duration = 7.0 h, stations New Norcia.
- ESA Delta-DOR: Quasar 664, one observation per day and per baseline. Two baselines used: Cebreros-New Norcia and Cebreros-Malargüe.
- Differenced Doppler using the same station combinations as for Delta-DOR, sampling rate 60 s, Doppler count time 60 s. The observations are scheduled during 2 hours, or the full common visibility period (with 15 degrees of minimum elevation) if smaller than 2 hours.

**Table 9: Schedule of ExoMars**  
(From Optimisation EXM LWO\_PROTON\_LAU\_TGO\_WALK\_IN)

Event	Date [TDB]	Delta-V [m/s]	Duration [s]
Begin of orbit file	2016/01/08 00:55:07.954		
Deep Space Maneuver 1	2016/05/18 04:35:08.837	569.950	5158.5
Deep Space Maneuver 2	2016/06/01 06:01:07.378	11.632	95.8
Separation Event	2016/10/16 12:09:00.962	0.0651	0.0

## 6.2. Applicability of Observation Types

**DTP:** As can be seen in Figure 6, the phase angle during the approach is of about 90 degrees, which assures enough magnitude of Mars as seen from the spacecraft to be detected by an on-board camera of similar type as the Rosetta’s NAVCAMs.

**SBI:** Similar to the MEX approach to Mars, the angle Mars-Earth-Probe is for most of the approach larger than the antenna beam width, see Figure 7. The SBI measurement availability with a hypothetical Mars orbiter is too late to be used.

**Landmarks:** To be able to recognize landmarks in the images, we assumed that Mars must extend in the images over a minimum size of 100 pixels, which corresponds to 0.5 degrees in the (Rosetta) NAVCAM. Figure 8 shows the evolution of this value during the approach. This size is achieved too late during the approach, so this observation type cannot be used either.

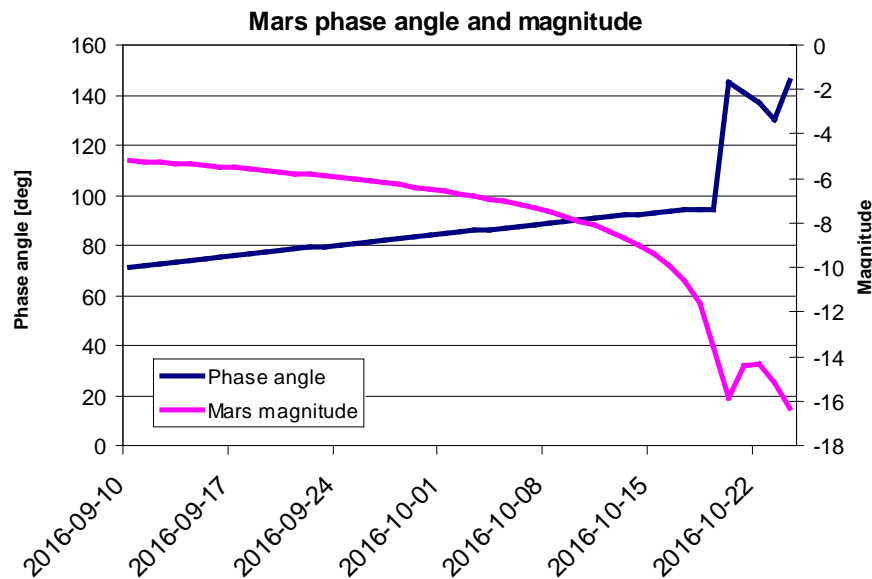


**Figure 6. Mars Phase Angle and Magnitude as Seen from EXM during Approach**

## 6.3. Models and Parameters

### Gravity and Solar Radiation Pressure

- Newtonian point mass acceleration due to the Sun, planets, Pluto, Moon and the three main asteroids: Ceres, Pallas and Vesta; 20x20 Mars gravity field expansion; Perturbative relativistic acceleration due to the Sun.
- Flat plate model with effective surface = 44.025 m<sup>2</sup>, mass 3596.0 kg.

### Uncertain OD Parameters

Assumed uncertainties are given in Table 10. For the purpose of this analysis the parameters marked as “C” are set as solve-for. In real operations they would probably be configured as consider parameters.

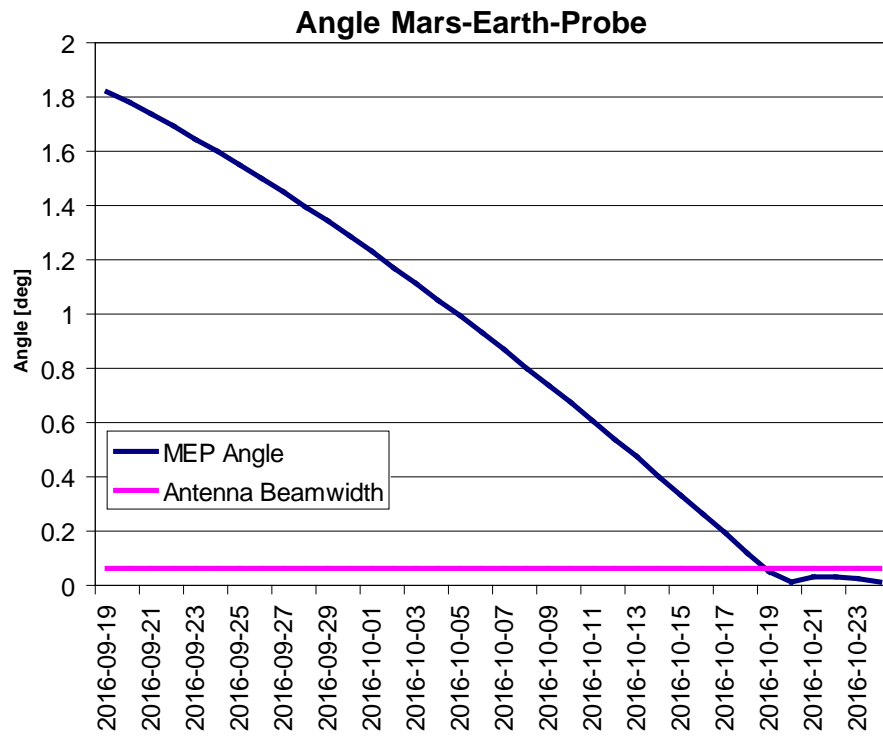


**Figure 7 Angle Mars-Earth-Probe and Antenna Beam Width Comparison (EXM)**

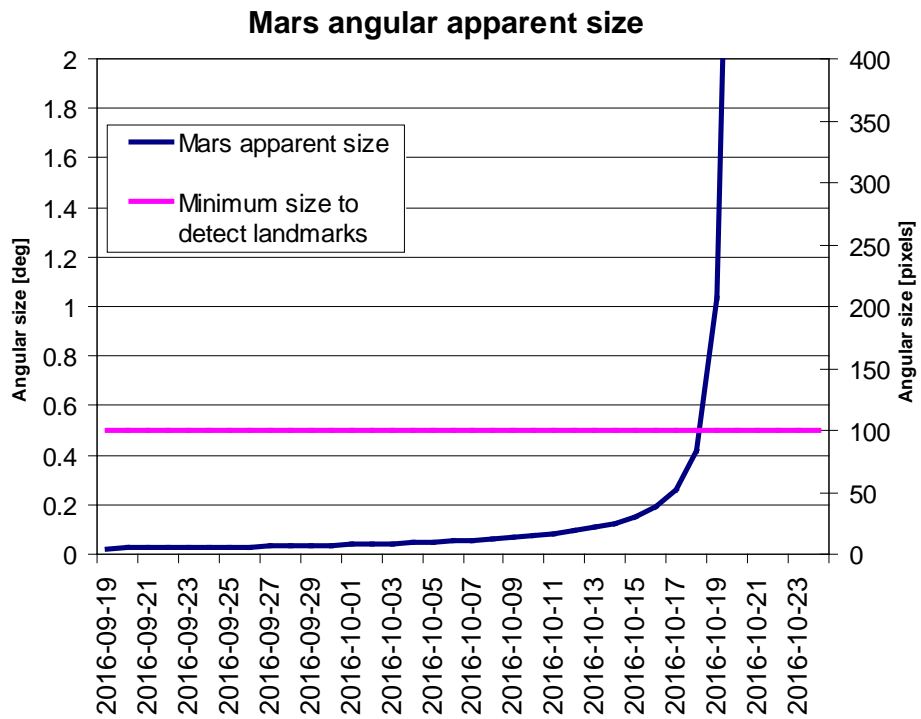


**Figure 8 Mars Angular Apparent Size as Seen from EXM**

**Table 10. Uncertain OD Parameters (EXM)**

OD parameter	Type	A priori value	1 $\sigma$ a priori uncertainty
Spacecraft state at epoch	S	taken from optimization orbit	1000 km, 100 m/s
Correction to Mars state at epoch	S	0, 0	1 km, 0.001 mm/s
SRP scale coefficient	S	+0 %	10 %
ESA station 1-way range bias per pass	S	0	0.02 km
Maneuvers	S	as optimized	3 % of acceleration for each direction in EME2000 frame (opt. acceleration file)
TCM-4	S	0.0	1.5 mm/s in each component (assuming 50 mm/s in this stochastic maneuver not included in optimization)
WOLs	S	0.0 in each component	0.5 mm/s in each component
ESA stations location	C	0	10 cm in each direction
Earth rotation parameters	C	0 0	30 nrad in pole error 0.75 ms in UTC-UT1
Troposphere calibration (zenith delay)	C	0 0	4 cm (wet part) 1 cm (dry part)
Ionosphere calibration scale factor	C	+0 %	25 %
Quasar 664 spherical coordinates correction	C	as provided in file icrf04	

**Measurements Noise**

Values in Table 11 are used as inputs for the observation scheduler. It is not clearly known which measurement noise value should be used for the differenced Doppler observable. However the difference Doppler noise is expected to be smaller than the 2-way Doppler noise because part of the media propagation effects are cancelled out when subtracting the measurements taken from the 2 stations (namely atmospheric and interplanetary plasma for the uplink and most interplanetary plasma for the downlink). To cover all possibilities, we tested different values for the noise sigma, in an interval from 0.2 m/s (2-way Doppler noise level) to 0.02 mm/s.

**Table 11: Measurement Noise for Each Observation Type (EXM)**

ID	Observation type	Noise sigma		Converted	
1	IFMS two/three way Range	1.667E-8	s	5.0	M
2	IFMS two/three way Doppler	6.667E-13		0.2	mm/s
10	ESA delta-DOR (s/c and quasar)	2.50E-001	ns		
14	Optical navigation (Mars center)				
	Right ascension	5E-3	deg	1	pixel
	Declination	5E-3	deg	1	pixel
	Correlation coefficient:	0.0			
16	IFMS differenced Doppler	6.667E-13		0.20	mm/s
		3.333E-13		0.10	mm/s
		1.667E-13		0.05	mm/s
		6.667E-14		0.02	mm/s

## 6.4. Comparison of Navigation Concepts

The concepts we tried are:

- Doppler only
- Range + Doppler
- Range + Doppler + Delta-DOR with baselines CEB-NNO and CEB-MLG
- Range + Doppler + Directions to Mars from optical images (DTP)
- Range + Doppler + DTP + Differenced Doppler.

As shown in Table 12 the Doppler only solution has very big uncertainties in both B-plane position and arrival time. Adding the range measurements already reduces a lot the uncertainties (by one order of magnitude). Of the two Delta-DOR baselines, CEB-NNO is the one that more reduces the position error, while CEB-MLG reduces more the time uncertainty. The full solution with all measurements provides an uncertainty of 24 km in B-plane position and 4.5 seconds in arrival time. Optical observations improve, but not by much, the solution when added to the Range + Doppler case. Differenced Doppler measurements improve quite a lot the solution when added to the Range + Doppler case. The obtained results are close (although worse) to the Range + Doppler + Delta-DOR case. Adding optical observations to the Range + Doppler + Differenced Doppler case improves only slightly the achieved uncertainty.

**Table 12: B-plane  $3\sigma$  Uncertainty Ellipse Parameters (EXM)**

Measurements combination	Semi-Major Axis [km]	Semi-Minor Axis [km]	Time Uncertainty [s]	Semi-Major Axis Angle [deg]
Doppler	1704.7	209.7	723.2	26.1
Doppler, Range	158.2	41.9	27.4	113.2
RG_DP_CEB-NNO DDOR	30.2	23.2	8.4	81.7
RG_DP_CEB-MLG DDOR	67.7	16.7	5.0	144.5
RG_DP_DDOR both baselines	24.2	15.4	4.5	137.3
RG_DP_Optical	132.2	33.0	23.5	111.6
RG_DP_DIDO_0.20	76.5	27.9	13.1	117.1
RG_DP_DIDO_0.20_Optical	71.0	25.7	12.3	116.3
RG_DP_DIDO_0.10	52.2	25.0	9.0	123.0
RG_DP_DIDO_0.10_Optical	48.5	23.5	8.6	121.8
RG_DP_DIDO_0.05	40.5	22.9	7.3	128.0
RG_DP_DIDO_0.05_Optical	37.5	21.7	6.9	127.3
RG_DP_DIDO_0.02	32.8	21.5	6.5	129.5
RG_DP_DIDO_0.02_Optical	30.7	20.5	6.2	129.4

For this scenario we can draw the following conclusions: From all tested configurations, the traditional radiometric navigation concept, Range + Doppler + Delta-DOR, provides the best knowledge on the B-plane position and arrival time. Optical measurements (as direction from the spacecraft to Mars center) are not so useful in this scenario, since they do not improve much the solution of range and Doppler only. On the other hand, Differenced Doppler combined with line

of sight measurements (Range and Doppler) results in a very interesting reduction of the B-plane uncertainties:

- With a Differenced Doppler sigma of 0.2 mm/s, the semi-major axis is reduced by half with respect to the Range + Doppler case. With a sigma of 0.1 mm/s the reduction is of one third, being the resulting ellipse roughly twice as big as the Delta-DOR one. This noise level seems quite likely to be achieved in real measurements, showing that differenced Doppler can be a very useful observation type for this scenario.
- For the case with the smaller used measurement sigma: 0.02 mm/s (unlikely to be achieved with real measurements), the obtained uncertainty is quite close to the Delta-DOR one, although still worse.

## 7. BepiColombo Mercury Magnetosphere Orbiter (MMO) Separation

This section analyses which orbital knowledge can be achieved until the MMO delivery. For the orbit insertion a series of 5 apocenter lowering maneuvers is planned from Burn 1 on January 1, 2024 (=8766 MJ2TDB) until delivery of the MMO on January 16. Table 13 gives the schedule of the approach and the orbital period achieved after each maneuver. The scenario uses the orbit and acceleration file from optimization `ins_mpo_6034_001_frc_mas_vals_hgm03`, which is based on [8]. The maneuvers consist of a liquid settling phase where the thrust is ramped up from 10 to 100% over 500 seconds and a burn firing phase with 100% thrust. Details of the MMO and MOSIF ejections are not modeled, instead they are assumed as impulsive maneuvers parallel to the velocity using spring energies of 1 J (value is place holder) for MMO and 29 J (value taken from literature) for MOSIF.

**Table 13: Schedule of Mercury Approach (BC)**

Event	Date [MJ2TDB]	Date [TDBCAL]	Delta-V [m/s]	Duration [s]	Period [h]
<b>Begin of orbit file</b>	8766.2802001121	2024/01/01_06:43:29.28969			326.4
Burn 1	8766.2935623614	2024/01/01 07:02:43.78802	60.4568918225	1898.911	71.6
Burn 2	8769.2437529884	2024/01/04 05:51:00.25820	64.4531288055	1973.110	32.9
Burn 3	8771.9776829584	2024/01/06 23:27:51.80761	76.7405417485	2259.380	18.4
Burn 4	8775.0495413392	2024/01/10 01:11:20.37171	89.5148458403	2534.286	11.6
Burn 5	8778.4316395947	2024/01/13 10:21:33.66098	54.4134558787	1591.543	9.3
<b>MMO Jettisoning</b>	8781.3533106525	2024/01/16 08:28:46.04038	0.0122935249	0.000	

### 7.1. Schedule

- The S/C a-priori state is taken at 2024/01/16 08:27:46.0 (MJD 8781.35261620) with Sigma 50 km, 5m/s, one minute before the start of the MMO separation, such that the results of the covariance analysis represent directly the orbital knowledge for the maneuver optimization and commanding. The state of Mercury is taken at the same time in order to allow relative values.
- Observation interval: 2024/01/13T10:48:06 to 2024/01/15T02:28:46.040, i.e. from end of the last apocenter lowering maneuver before the MMO separation up to a data cut-off 30 hours before the MMO separation

- ESA-2-Way Range: X-band, sampling rate 1200 s; ESA-2-Way Doppler: X-band, sampling rate 60 s, Doppler count time 60 s; Both with minimum elevation = 15.0 deg, pass duration = 6.0 h, stations 74 (New Norcia), 83 (Cebreros), and 84 Malargüe.
- ESA-Delta-DOR: Quasar 664, pass frequency 1, baseline 1 with stations 74 and 83 (New Norcia and Cebreros), baseline 2 with stations 83 and 84 (Cebreros and Malargüe).
- Differenced Doppler using the same station combinations as for Delta-DOR, Sampling rate 60 s, Doppler Count time 60 s, pass duration 6 h.

## 7.2. Applicability of Observation Types

**Delta-DOR:** The usage of Delta-DOR may be difficult because of Mercury’s close proximity to the Sun. For the current trajectory one candidate quasar (Number 664) and one defining quasar (Number 486) could be found. We used 664, but established that it could be exchanged with 486 without significant changes of the results.

**DTP and Landmarks:** Usage of the cameras for navigation will be impossible while the field of view is blocked by MOSIF/MMO. On top of that the S/C follows during the approach in its approach configuration (MPO + MOSIF + MMO) for thermal reasons a complicated rotation pattern around axes which renders any attempt to use a camera virtually impossible.

**SBI:** Not applicable as there is no 2<sup>nd</sup> spacecraft available.

## 7.3. Models and Parameters

### Gravity and Solar Radiation Pressure

- Newtonian point mass acceleration due to Sun, planets, Pluto, Moon, 50x50 field expansion (grav\_mercury\_hgm003b) for Mercury with perturbative relativistic acceleration due to the Sun
- Flat plate model with effective surface = 14.00 m<sup>2</sup>, mass 2250.00 kg

### Uncertain OD Parameters

Maneuvers before the data cut-off are included as solve for, while maneuvers thereafter are taken as exact. Consider parameters are switched off. When switched on, or assumed as solve-for parameter, we assume the uncertainties as given in Table 14.

### Measurements Noise

Values in Table 6 for IFMS Range (ID 1), Doppler (ID2), Delta\_DOR (ID 10), and Differenced Doppler (ID 16) are used as inputs for the observation scheduler. For Differenced Doppler a number of computations are repeated with a higher estimate of 3.33E-13 (0.1 mm/s) for the Noise sigma. Below the associated computations are marked with a “\*”.

**Table 14: Uncertain OD Parameter (BC)**

OD parameter	Typ	A priori value	1 $\sigma$ a priori uncertainty
Spacecraft state at epoch	S	taken from optimisation	50 km, 5 m/s
Solar radiation pressure	S	0.0	5 %

OD parameter	Typ	A priori value	1 $\sigma$ a priori uncertainty
coefficient			
TCM	S	as optimized	3 % of acceleration for each direction in EME2000 frame (using acceleration file of optimization)
ESA stations location	C	0	10 cm in each direction
ESA station 1-way range	C	0	0.02 km
Quasar directions	C	file icrf04	
Troposphere calibration (zenith delay)	C	0 0	4 cm (wet part) 1 cm (dry part)
ionosphere calibration scale factor	C	+ 0 %	25 %
Mercury ephemeris position, velocity	C	0	1 km, 0.01 mm/s
Mercury gravity constant $\mu$	C	0	0.01 km**3/s**2

#### 7.4. Comparison of Navigation Concepts

The concepts we tried are:

- Doppler only
- Range + Doppler
- Range + Doppler + Delta-DOR
- Range + Doppler + Differenced Doppler
- Range + Doppler + Delta-DOR + Differenced Doppler.

Table 15 shows the  $1\sigma$ -uncertainty of the a posteriori spacecraft state directly before the MMO separation. To obtain the covariance analysis results, the maximum uncertainties in position and velocity are extracted from the uncertainty ellipsoid for the state at epoch, 2024/01/16 08:27:46.0 (MJD 8781.35261620), which corresponds to the date of the a-priori state. The table also shows the volume of the position uncertainty ellipsoid and the uncertainties of the keplerian spacecraft state components in Earth equatorial J2000.0 system, centered at Mercury. “Without” in the table means that types for the S/C state and the solar radiation pressure acceleration coefficient are set as solve-for parameters while TCMs and all other parameters of Table 14 are taken as exact, “Consider” means that types for the S/C state, the solar radiation pressure acceleration coefficient and the TCMs are set as solve-for parameters while all other parameters are taken as consider parameters, “Solve-For” means that all parameters are taken as solve-for parameters.

Position and velocity errors of the “Consider” case in Table 15 are large because they are affected by the large uncertainty assumed for the ephemeris of Mercury. Especially the Mercury position uncertainty has the largest contribution to the state and velocity errors in all combinations.

The volume of the solve-for position error ellipse shows a large effect of the Range measurement when added to Doppler, but otherwise it reflects mainly what can be seen in the position maximum errors. Zero volumes result from components of the position error being zero.

**Table 15: Results for Concepts (BC)**

Case:	Position	Velocity	Volume	A	E	I	RAAN	Arg. Per.	True Anom.
	(km)	(mm/s)	(km <sup>3</sup> )	(km)		(deg)	(deg)	deg)	(deg)
<b>Without</b>									
DP	1.00E-02	2.10E+00	0.00E+00	8.56E-06	3.02E-09	1.45E-04	5.49E-05	2.92E-05	2.21E-07
RG_DP	9.90E-03	2.10E+00	0.00E+00	8.54E-06	3.00E-09	1.45E-04	5.47E-05	2.91E-05	2.20E-07
RG_DP_DDOR	9.90E-03	2.10E+00	0.00E+00	8.54E-06	3.00E-09	1.45E-04	5.47E-05	2.91E-05	2.20E-07
RG_DP_DDOR_DIDO	9.90E-03	2.10E+00	0.00E+00	8.49E-06	2.99E-09	1.44E-04	5.44E-05	2.90E-05	2.19E-07
RG_DP_DIDO	9.90E-03	2.10E+00	0.00E+00	8.49E-06	2.99E-09	1.44E-04	5.44E-05	2.90E-05	2.19E-07
<b>Consider</b>									
DP	1.00E+00	2.70E+00	4.18E+00	7.40E-01	2.53E-05	1.67E-03	3.78E-03	6.35E-03	2.25E-03
RG_DP	3.16E+00	5.97E+02	3.96E+00	7.37E-01	2.63E-05	4.20E-02	1.56E-02	1.03E-02	2.24E-03
RG_DP_DDOR	3.16E+00	5.97E+02	3.96E+00	7.37E-01	2.63E-05	4.20E-02	1.56E-02	1.03E-02	2.24E-03
RG_DP_DDOR_DIDO	3.13E+00	5.89E+02	3.96E+00	7.37E-01	2.63E-05	4.15E-02	1.54E-02	1.02E-02	2.24E-03
RG_DP_DIDO	3.13E+00	5.90E+02	3.96E+00	7.37E-01	2.63E-05	4.15E-02	1.54E-02	1.02E-02	2.24E-03
<b>Solve-For</b>									
DP	9.96E-01	2.30E+00	4.16E-02	2.51E-01	8.42E-06	1.69E-04	1.56E-04	6.22E-03	2.21E-03
RG_DP	9.51E-01	2.30E+00	1.10E-03	4.81E-02	1.31E-06	1.68E-04	1.40E-04	6.00E-03	2.13E-03
RG_DP_DDOR	9.13E-01	2.30E+00	1.05E-03	4.62E-02	1.26E-06	1.67E-04	1.40E-04	5.76E-03	2.05E-03
RG_DP_DDOR_DIDO	8.97E-01	2.20E+00	1.04E-03	4.54E-02	1.23E-06	1.65E-04	1.38E-04	5.66E-03	2.01E-03
RG_DP_DDOR_DIDO*	9.09E-01	2.30E+00	1.04E-03	4.59E-02	1.25E-06	1.66E-04	1.39E-04	5.73E-03	2.04E-03
RG_DP_DIDO	9.46E-01	2.20E+00	1.10E-03	4.78E-02	1.30E-06	1.65E-04	1.39E-04	5.96E-03	2.12E-03
RG_DP_DIDO*	9.49E-01	2.30E+00	1.09E-03	4.80E-02	1.30E-06	1.66E-04	1.39E-04	5.99E-03	2.13E-03

The increase of the Differenced Doppler noise sigma by a factor 5 (marked by “\*\*”) leads to an increase of the position and velocity errors of the basic type by roughly factors 2.8 and 2.4, respectively, for the case “Solve-For”, but in combinations with Range and Doppler the factors are close to 1.0, showing a minor influence of this noise sigma on the overall errors.

The combination Range + Doppler + Delta-DOR + Differenced Doppler reduced the position error in Tab. 15 from using Doppler alone by about 10%. The error level obtained in this observation arc is at 900 m in position and 2.3 mm/s in velocity.

The overall effect of the Differenced Doppler measurements on the position error appears to be minor compared to the standard Range + Doppler and Range + Doppler + Delta-DOR combinations. From above combinations only Differenced Doppler leads to a further reduction of the velocity errors by 4% compared to pure Doppler and this only in case a very small error sigma of 0.02 mm/s is assumed, which is a factor 10 smaller than that of Doppler. Minor effects can be seen in all keplerian elements.

A repetition of above computations with an observation arc extended by 6 hours (for changes in the operations timeline) had only minor influence on the position and velocity errors in all combinations. Further experiments with the observation duration, where the begin of the observation arc was extended to earlier times, showed for all combinations position errors below 1 km and velocity errors below 3 mm/s once the duration was longer than 2 days.

## 8. Rosetta Relay Phase

During the Relay Phase, which starts after the Lander Delivery Phase, Rosetta establishes a communications link Philae-Rosetta-Earth and acts as communication relay for the lander Philae. The Rosetta trajectory during this phase is designed to maximize the visibility periods. We analyzed, how adding the knowledge of the Rosetta relative orbit around the comet during the Relay Phase can be improved by orbiter-lander tracking observations (in this case 1-way Doppler). Table 16 shows the schedule of both Lander Delivery and Relay phases. The scenario uses the orbit and acceleration file of optimization 130206\_CompleteTrajectory\_orbiter.

**Table 16: Schedule of Lander Delivery and Relay phases (ROS)**

Event	Date [TDB]	Delta-V [mm/s]	Duration [s]
Begin of orbit file	2004/03/02 09:26:21.583		
Begin of Lander Delivery Phase	2014/10/26 09:00:00.000		
SDP-1 Maneuver	2014/10/26 09:01:07.182	57.7	4.8
SDP-2 Maneuver	2014/10/31 16:00:00.000	75.4	6.3
SDP Predelivery Maneuver	2014/11/11 14:22:09.287	913.0	75.7
SSP Separation	2014/11/11 16:53:25.018	30.9	0.0
SDP Postdelivery Maneuver	2014/11/11 17:23:25.018	800.0	62.3
Begin of Relay Phase			
RP-1 Maneuver	2014/11/12 01:01:07.183	835.0	64.9
RP-2A Maneuver	2014/11/16 09:01:07.183	150.9	11.7
RP-2B Maneuver	2014/11/16 13:01:18.917	222.9	17.3
Begin of Extended Monitoring Phase	2014/11/19 09:01:07.183		

The operational approach for the lander delivery phase is that the whole sequence containing pre-delivery maneuver, lander separation, post-delivery and RP-1 maneuvers is commanded in the last Flight Dynamics cycle. After the execution of these maneuvers, the relative state knowledge is degraded by maneuver errors and COMA drag mismodeling. The scenario analyzed now comprises the first orbit determination to be performed in this phase, to prepare for optimization and commanding of the RP-2 A and B maneuvers, which are intended to maintain the orbiter in a trajectory that maximizes the lander visibility times. This is achieved by keeping the spacecraft comet-centric latitude in an interval centered in the latitude of the landing site.

For the landmark observations we assumed that the navigation cameras are used, since they are the baseline for navigation. However, Rosetta carries 2 more optical cameras, the OSIRIS scientific instrument, which could be used in case they are available. Properties of the cameras are taken from [9] and are summarized in Table 3. One image every 4 hours is assumed for this phase, where we use a randomly simulated landmark database with a variable number of landmarks, following a uniform probability distribution on the comet surface (assumed spherical). The observation scheduler checks whether a landmark is visible from the spacecraft with a minimum emission angle, whether it is in the day side of the comet, and whether it falls inside the camera field of view.

## 8.1. Schedule

- Observation interval: 2014/11/11\_18:00 - 2014/11/13\_03:00. Data cut-off following the current planning defined in the VSPL timeline. The observation start time is taken right after the post-delivery maneuver execution, so that the events happened before (maneuvers and lander delivery) are not calibrated for their effect on the S/C velocity. The RP-1 maneuver falls inside the observation arc and is thus calibrated.
- The S/C orbit, comet orbit and attitude a-priori states are taken at the end of the arc, 2014/11/13 03:00, with very big uncertainties so that the run results represent the amount of information obtained from the measurements.
- ESA-2-Way Range: X-band, sampling rate 1200 s, ESA-2-Way Doppler: X-band, sampling rate 60 s, Doppler count time 60 s, both with minimum elevation = 15.0 deg, pass duration = 7.0 h, station New Norcia.
- Spacecraft to Lander 1-Way Doppler: Sampling rate and Doppler count time 60 s. Minimum elevation of the spacecraft as seen from the lander 30 degrees in order to account for the lander antenna beam width (60 degrees of semi-angle).

## 8.2. Models and Parameters

### Gravity and Solar Radiation Pressure

- Newtonian point mass acceleration due to the comet, Sun, planets, Pluto, Moon and the three main asteroids: Ceres, Pallas and Vesta; 4x4 comet gravity field expansion; Perturbative relativistic acceleration due to the Sun.
- Flat plate model with effective surface = 90.048 m<sup>2</sup>, mass 1483.219 kg.

### Coma Drag

- Engineering coma model with spacecraft as cannon ball with 67 m<sup>2</sup> of cross-surface.

### Uncertain OD Parameters

Assumed uncertainties are given in Table 17. For the purpose of this study the consider parameters (type C) are also set as solve-for.

### Measurements Noise

Values in Table 6 for IFMS Range (ID 1), Doppler (ID 2) and optical landmarks navigation (ID 15) were used as inputs for the observation scheduler. The noise of Spacecraft-lander tracking (ID 19) was varied as explained below.

**Table 17: Uncertain OD Parameters (ROS)**

Solve-for parameters	Typ	A priori value	1 $\sigma$ a priori uncertainty
Spacecraft state at epoch	S	taken from optimization orbit	1000 km, 100 m/s
Comet state at epoch	S	taken from determined orbit using astrometric observations from ground	1000 km, 100 m/s
Comet attitude state at epoch	S	taken from comet reference model	Full freedom in initial quaternion, 1.0D-6 rad/s in angular rates
Comet inertia matrix	S	Identity matrix	0.1 kg/km <sup>2</sup>

Solve-for parameters	Typ	A priori value	1 $\sigma$ a priori uncertainty
Comet mu	S	8.067722D-7 km <sup>3</sup> /s <sup>2</sup>	1.0D-7 km <sup>3</sup> /s <sup>2</sup>
COMA drag scale coefficient	S	+0 %	100%
SRP scale coefficient	S	+0 %	10%
ESA station 1-way range bias per pass	S	0	0.02 km
Maneuvers	S	as optimized	3 % of acceleration for each direction in EME2000 frame (using acceleration file of optimization)
WOLs	S	0.0 in each component	1 mm/s in each component
Lander coordinates in comet-fixed frame	S	from optimization	1 km in each component
Landmark coordinates	S	from simulated DB	variable (see below)
Image orientation calibration	S	0	20 mdeg in image vertical and horizontal directions
ESA stations location	C	0	10 cm in each direction
Earth rotation parameters	C	0 0	30 nrad in pole error 0.75 ms in UTC-UT1
Troposphere calibration (zenith delay)	C	0 0	4 cm (wet part) 1 cm (dry part)
Ionosphere calibration scale factor	C	+0 %	25 %

### 8.3. Configurations

For landmarks four randomly simulated landmark databases (identifiers and coordinates in comet-fixed frame) containing 25, 50, 75 or 100 landmark positions are used. A minimum angular separation between the landmarks is imposed to assure that the whole comet surface is covered. In this mission phase the landmarks coordinates are assumed to be accurately known. To measure the effect of the landmark coordinate uncertainty in the OD performance, three different values are tested for the a-priori 1-sigma uncertainty in each component: 100 m, 10 m and 1 m.

In the time interval covered, the spacecraft is at about 25 km of the comet. At this distance, the comet totally fills the camera Field of View (FOV), even using the Wide Area Camera (WAC) it could not be assured that the full comet is captured in an image. Therefore, the number of known landmarks plays an important role in the OD accuracy. To check their effect, the camera FOV has been varied. NAVCAMs have a rectangular FOV of 5x5 degrees, which has been modeled as a cone FOV with semi-angle of 3 degrees, but we also used 6 deg to cover the case that OSIRIS-WAC is used, or that 4 raster images are taken using the NAVCAM.

Since there is not an established value for the measurement noise of the spacecraft-lander 1-way Doppler observable, different values have been tested in an interval from 20 m/s to 0.2 m/s with a step of a factor of 10 between each value.

We performed 168 covariance analysis runs for the navigation concepts Range + Doppler + Landmarks and Range + Doppler + Landmarks + Spacecraft-Lander Tracking, covering all

combinations of values of the varying parameters: number of landmarks, a-priori landmark position uncertainty, camera FOV, and spacecraft-lander tracking measurement sigma. We compared the results of these runs in terms of the a posteriori uncertainty in spacecraft-comet relative state (as maximum error in position and velocity). Additionally, we also compared for the runs with spacecraft-lander tracking the a posteriori uncertainty in the lander coordinates. To obtain the covariance analysis results, we extracted the maximum 1-sigma uncertainties in relative position and velocity from the uncertainty ellipsoid printout for the state at epoch.

#### 8.4. Comparison of Navigation Concepts

With measurement sigma for spacecraft-lander tracking higher than 20 mm/s, this measurement does not add much information to the spacecraft relative state. For the best case, with 0.2 mm/s (same as Doppler tracked from ground) the spacecraft state knowledge is improved by a factor of at most 2 in all cases. With measurement sigma for spacecraft-lander tracking higher than 2 m/s, this measurement does not contain enough information to reduce the a priori uncertainty on the lander coordinates. With a sigma of 20 mm/s, or smaller, the improvement is quite significant.

In all cases, the obtained lander coordinates estimation accuracy is strongly related with accuracy in the estimation of comet attitude, which is mainly obtained from the landmark observations. Therefore the more and better landmark observations the better lander coordinate estimation is achieved with the spacecraft-lander tracking. We noticed, that the addition of lander tracking observations does neither improve much the uncertainty in comet attitude parameters nor in landmark coordinates with respect to the landmark only case. A similar pattern is repeated in the results of all combinations of number of landmarks, a priori landmark position uncertainty and camera FOV, scaled with the a posteriori knowledge on the comet attitude obtained in the landmark observations only case.

Figure 9 shows the obtained relative Spacecraft state uncertainty as a function of used spacecraft-lander measurement sigma (the curve of landmark only case is constant, since this observation type is not used), Figure 10 the same for the lander coordinates. Only the results for two selected cases are shown:

- Best case: corresponds to the case where the landmarks-only solution provides the best relative state knowledge: biggest number of landmarks (100), smallest a priori sigma in landmark position (1m) and biggest FOV are used (6 deg).
- Worst case: with 25 landmarks, biggest a priori sigma in landmark position (100m), and smallest FOV (3 deg).

From the results it can be observed that the spacecraft-lander tracking observations contain information on the spacecraft-comet relative state and the lander coordinates. However, a very small measurement sigma is required for this information to be strong enough to reduce the uncertainty obtained with the landmarks only observations navigation concept. Such a small measurement sigma is probably unfeasible in a real mission, due to the instabilities of spacecraft and lander clocks. On the other hand, this observation type has proved to be useful to refine the lander coordinate estimates. A significant improvement is already achieved with sigmas of 2 m/s or 200mm/s, depending on the case.

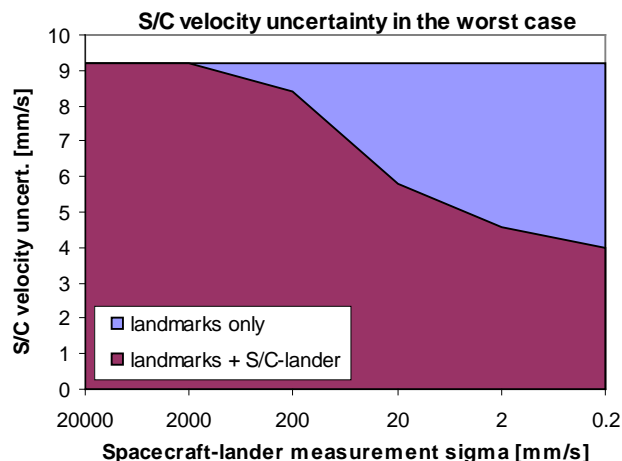
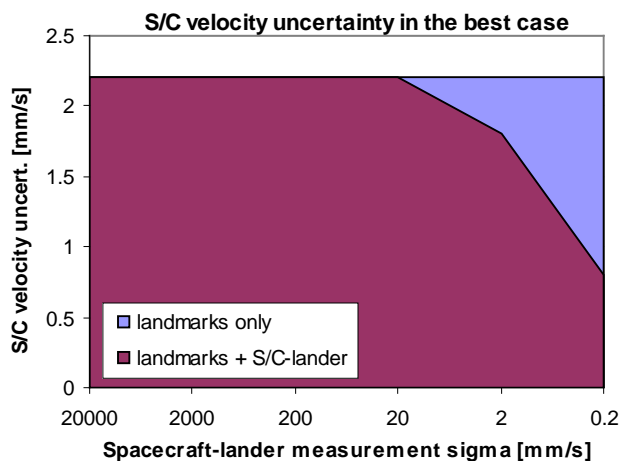
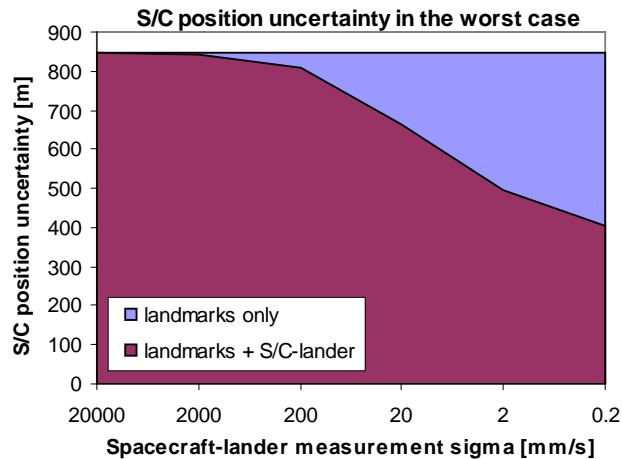
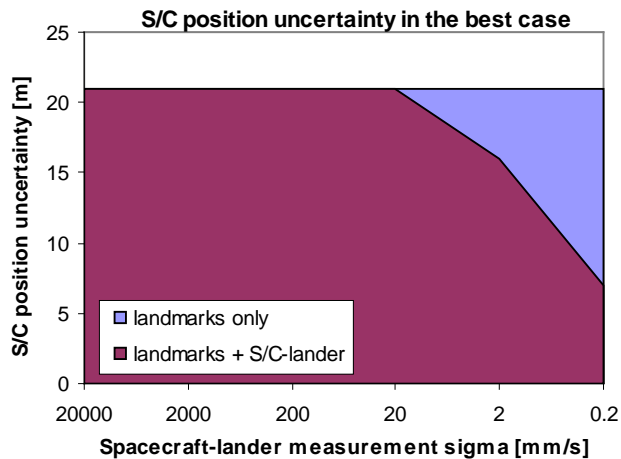


**Figure 9. Results of Relative S/C Position Uncertainty for 2 Selected Cases (ROS)**

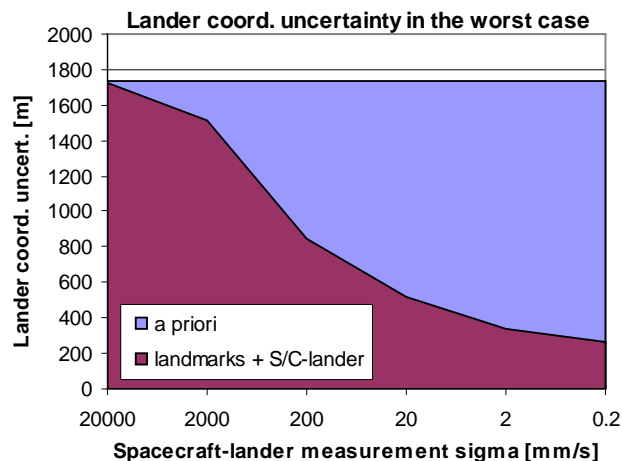
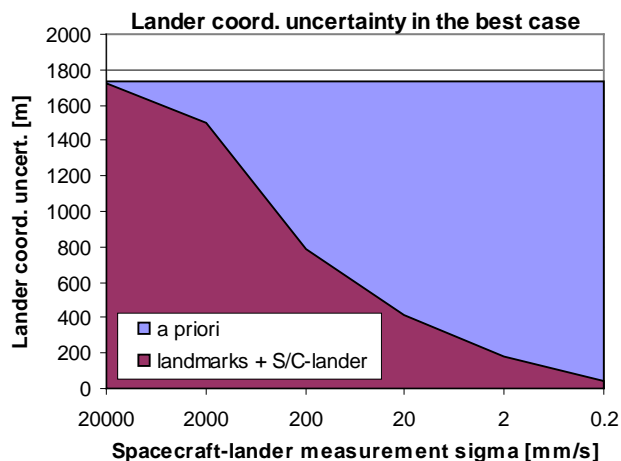


**Figure 10. Results of Relative Lander Coordinates Uncertainty for 2 Selected Cases (ROS)**

## 9. Conclusions

- In all considered scenarios the combination Range + Doppler + Delta-DOR gives the lowest errors in case two baselines with large direction differences can be used.
- In case a 2nd spacecraft is present, the combination of Range and Doppler with S/C-S/C Doppler can provide comparable accuracy, even more if also combined with DTP.
- The S/C lander data type has proved to be useful to refine lander coordinate estimates.
- The possibility to use SBI in a planetary approach is limited, because both S/C appear too late together inside the antenna beam to be relevant for the orbit insertion commanding.
- To be able to recognize landmarks in the images, we assumed that Mars must extend in the images over a minimum size of 100 pixels, which corresponds to 0.5 degrees in the Rosetta NAVCAM. This size is achieved too late during an approach so this observation type cannot be used either.
- Differenced Doppler combined with line of sight measurements (range and Doppler) may result in significant reductions of the B-plane uncertainties w.r.t. Range + Doppler case. In the ExoMars scenario, for example, with a Differenced Doppler sigma of 0.1 mm/s the reduction is of one third, resulting in an error ellipse roughly twice as big as with the combination Range + Doppler + Delta-DOR.

## 10. References

- [1] Bauske, R. "Final Report", ESA Study 4000100260/10/D/JR "New Concepts for Relative Navigation at Planetary Approach", Darmstadt, Germany, 2013.
- [2] Casotto, S. "Interplanetary Tracking Measurements Models and Observation Equations" Technical Note of ESA Study 4000100260/10/D/JR "New Concepts for Relative Navigation at Planetary Approach", Darmstadt, Germany, 2011.
- [3] Thurman, S. W. "Deep Space Navigation with Differenced Data Types, Part II: Differenced Doppler Information Content" TDA Progress Report 42-103, Jet Propulsion Laboratory, Pasadena, California, 1990.
- [4] Morley, T., et al. "Mars Express Navigation for Beagle 2 separation and Mars orbit insertion" in Proceedings of the "18th International Symposium of Flight Dynamics", Munich, Germany, 2004.
- [5] Folkner, W. M. "DSN Station Locations and Uncertainties" TDA Progress Report 42-128, Feb. 15, 1997.
- [6] Conally, M. J. "Radio Source Catalog", DSMS Telecommunications Link Design Handbook, 810-005, Rev. E, 107, NASA/DSN, May 2006.
- [7] Khan, M. and Yamaguchi, T. "ExoMars, 2016 Mission, Consolidated Report on Mission Analysis", EXM-MS-RP-ESA-00008, Issue 4 Rev. 0, 2013-03-27
- [8] Jehn, R. and Schuster, A. "Orbit insertion and orbit evolution of BepiColombo's MPO and MMO spacecraft", MAS Technical Note No. 86, BC-ESC-RP-50008, Iss. 1.1, ESOC, Darmstadt, Germany, May 2013.
- [9] Munoz, P., et al "Preparations and Strategy for Navigation during Rosetta Comet Phase", Proceedings 23rd International Symposium on Space Flight Dynamics - 23rd ISSFD, Pasadena, USA, 2012.